IOP Publishing Journal of Physics B: Atomic, Molecular and Optical Physics
J. Phys. B: At. Mol. Opt. Phys. **53** (2020) 045402 (8pp) https://doi.org/10.1088/1361-6455/ab590c

Generation, control, storage and retrieval of complicated shaped four-wave mixing signal

Nawaz Sarif Mallick[1] **and Tarak Nath Dey**

Department of Physics, Indian Institute of Technology Guwahati, Guwahati, Assam 781039, India

E-mail: nawaz.phy@gmail.com and tarak.dey@iitg.ac.in

Received 21 May 2019, revised 11 November 2019
Accepted for publication 19 November 2019
Published 24 January 2020

Abstract

We present an efficient scheme for the generation and control of a non-degenerate four-wave mixing (FWM) signal in an *N*-type inhomogeneously broadened ^{87}Rb atomic system. We observe the propagation dynamics of the generated FWM signal along with the probe pulse under the condition of electromagnetically induced transparency. The FWM signal acquiring the scaled shape of the probe field travels through the medium without changing its shape and intensity. We have also shown that a time-dependent control field permits the storage and retrieval of these optical signals without losing their identity. This work allows us to generate, control, store and retrieve FWM signals of complicated shape.

Keywords: four-wave mixing, electromagnetically induced transparency, coherent optical effect

(Some figures may appear in colour only in the online journal)

1. Introduction

Atomic coherence induced by coherent light–matter interaction has a significant role in the precise control of the optical property of a medium. The observation of atomic coherence in an atomic system leads us to uncover many spectacular optical effects. Among the most well-known effects is electromagnetically induced transparency (EIT) [1, 2], in which an opaque medium becomes eminently transparent for the probe field with the support of a control field. Diverse applications such as slowing and stopping of light [3–5], coherent storage and retrieval of light [6–9], Rydberg blockade-induced interactions [10], diffraction control and guiding of light [11, 12], structured beam generation [13, 14], etc have been documented using EIT. In a multi-level atomic system, EIT enhances the nonlinear susceptibility, which conducts us to use the nonlinear optical regime in the investigation of many nonlinear optical phenomena such as Kerr nonlinearity [15, 16], self-phase modulation [17], cross-phase modulation [18, 19], and four-wave mixing (FWM) [20–23]. In the FWM process, three electromagnetic fields interact in a nonlinear optical system and generate an electromagnetic field with a new frequency. Numerous experiments have been carried out to demonstrate the enhanced FWM process in multi-level atomic systems [24–29]. The FWM process using EIT has been observed in both cold [30, 31, 26–29] and room-temperature [25, 32] atomic systems. Besides the FWM process, enhanced higher-order multi-wave mixing processes have been studied [33]. Kang *et al* experimentally demonstrated an EIT-based six-wave mixing signal in an *N*-type cold atomic system [34]. Recently an experimental observation of an FWM signal in an *N*-type cold atomic system has been studied by Chiu *et al* at low light levels [35]. Aside from the atomic system, various hybrid systems composed of semiconductor quantum dots and metallic nanoparticles or a photonic crystal nanocavity have been used to study the FWM process [36, 37].

The four-level system not only generates new signals, it also permits the generated signal to propagate through the nonlinear medium along with the probe field under the condition of EIT [31, 35]. The effect of enhanced nonlinearity on these propagating signals through the atomic medium remains unexplored. In addition, the shape of the generated FWM signal and the progression during its propagation through the inhomogeneously broadened medium is not completely elucidated. In this paper, we theoretically investigate all of these questions in a simple four-level *N*-type atomic configuration as shown in figure 1. Two weak probe fields and a strong control field resonantly drive the system. In order to efficiently generate an FWM signal, it is essential that the

[1] Author to whom any correspondence should be addressed.

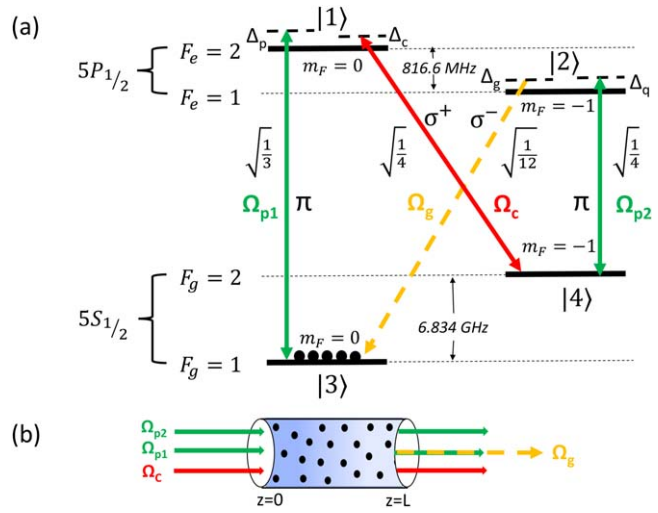

Figure 1. (a) Schematic representation of the proposed *N*-type atomic energy levels of ^{87}Rb D_1-line transition. The two metastable ground states are defined as $|3\rangle = |F_g = 1, m_F = 0\rangle$ and $|4\rangle = |F_g = 2, m_F = -1\rangle$. The two excited states are defined as $|1\rangle = |F_e = 2, m_F = 0\rangle$ and $|2\rangle = |F_e = 1, m_F = -1\rangle$. Two probe fields ($\Omega_{p1}$ and Ω_{p2}) and one control field generate an FWM signal with frequency $\omega_g = \omega_{p1} - \omega_c + \omega_{p2}$. The square root terms are the coupling strengths (Clebsch–Gordan coefficient) of the corresponding transitions. (b) A simple illustration of the model system.

phase-matching condition, $\vec{K}_{p1} + \vec{K}_{p2} = \vec{K}_c + \vec{K}_g$ is strictly fulfilled [25]. Here we conceive this by using a collinear geometry which generates the FWM signal in the same direction as the probe field propagates. The steady state of the optical Bloch equations is numerically solved to study the atomic coherence created by the nonlinear atom–field interaction. The numerical result clearly shows gain in the FWM spectrum which indicates the possibility of signal generation. The frequency of the signal, ω_g, is related to the frequency of the probe fields, ω_{p1} and ω_{p2}, and the frequency of the control field, ω_c, by $\omega_g = \omega_{p1} - \omega_c + \omega_{p2}$. Note that the difference between two probe frequencies, i.e. $\Delta\omega_p = \omega_{p1} \sim \omega_{p2} \ll \Delta\omega_{EIT}$, must be well contained within the EIT window, otherwise the probe pulses will suffer distortion from different absorption and group velocity dispersion. Hence, the generated FWM signal will also suffer the same kind of distortion due to the different gain and group velocity dispersion.

Apart from the generation and control of the FWM signal, the storage and retrieval of this signal along with the probe has captivated enormous attention due to its potential application as an optical memory [38–42]. Recently, many experiments have demonstrated simultaneous storage and retrieval of both the signals in a multi-level atomic system [40, 41, 43]. But the correlation between the input and the output pulse shape has not yet been explored in detail. It is noticeable from the previous demonstrations that the retrieved FWM signal does not preserve its predefined shape, and in addition its intensity is reduced considerably. We overcome these limitations by considering a non-degenerate atomic system in which two probe and one control field are interacting nonlinearly. In this paper we demonstrate the shape-preserving storage and retrieval of the FWM signal without compromising its intensity. We also find that the storage and retrieval process is robust with both adiabatic and non-adiabatic switching of the control field.

The arrangement of this article is as follows. In section 2.1, we configure the physical model and describe the system using semiclassical theory. In section 2.2, we discuss the dynamical equations of motion for the *N*-type system using Liouville's equation. In section 2.3, we derive the pulse propagation equations for the optical fields. In section 3, we investigate the generation and control of the FWM signal. In section 4, the storage and retrieval of the FWM signal is demonstrated. In section 5, we derive the analytical expression of the nonlinear coherence under weak probe approximation in order to explain the FWM scheme. Finally, in section 6, we briefly conclude our work.

2. Theoretical model

2.1. Model configuration

In this work, the four-wave mixing mechanism has been exploited for the generation and control of an optical signal. The model system consists of an inhomogeneously broadened four-level ^{87}Rb atomic system interacting with three co-propagating optical fields as shown in figure 1. The atomic transitions $|1\rangle \leftrightarrow |3\rangle$ and $|2\rangle \leftrightarrow |4\rangle$ are coupled by two probe fields of frequency ω_{p1}, ω_{p2} whereas a strong control field with frequency ω_c couples the $|1\rangle \leftrightarrow |4\rangle$ transition. These optical fields are defined as

$$\vec{E}_j(z, t) = \hat{e}_j \mathcal{E}_{0j}(z, t) e^{i(k_j z - \omega_j t)} + c.c.\,, \tag{1}$$

where $\mathcal{E}_{0j}(z, t)$ is the space-time-dependent amplitude, $k_j = \omega_j/c$ is the propagation constant in the z-direction and $\hat{e}_j$ is the polarization unit vector of the optical field. The subscript $j \in \{p1, p2, c\}$ indicates the two probe fields and control field, respectively. The Hamiltonian describing the interaction between the four atomic level system with the two optical fields under electric-dipole approximation is as given below

$$\begin{aligned} H' = {} & \hbar\omega_{13}|1\rangle\langle 1| + \hbar(\omega_{13} - \omega_{14})|4\rangle\langle 4| \\ & + \hbar(\omega_{13} - \omega_{14} + \omega_{24})|2\rangle\langle 2| - \hbar\Omega_{p1} e^{-i\omega_{p1}t}|1\rangle\langle 3| \\ & - \hbar\Omega_c e^{-i\omega_c t}|1\rangle\langle 4| - \hbar\Omega_{p2} e^{-i\omega_{p2}t}|2\rangle\langle 4| + h.c\,., \end{aligned} \tag{2}$$

where the Rabi frequencies of the probe and control are defined by

$$\Omega_{p1} = \frac{\hat{d}_{13}.\hat{e}_{p1}}{\hbar}\mathcal{E}_{0p1};\ \ \Omega_{p2} = \frac{\hat{d}_{24}.\hat{e}_{p2}}{\hbar}\mathcal{E}_{0p2};\ \ \Omega_c = \frac{\hat{d}_{14}.\hat{e}_c}{\hbar}\mathcal{E}_{0c}$$

The dipole moments for the atomic transitions between states $|1\rangle \leftrightarrow |3\rangle, |2\rangle \leftrightarrow |4\rangle$ and $|1\rangle \leftrightarrow |4\rangle$ are denoted by $\hat{d}_{13}$, $\hat{d}_{24}$ and $\hat{d}_{14}$, respectively. Note that the Clebsch–Gordan coefficients of the considered level scheme, $|\hat{d}_{13}|/|\hat{d}_{24}| = \sqrt{4/3}$,

approximately imply that $|\hat{d}_{13}| \approx |\hat{d}_{24}|$ [26, 35, 43–45]. So, we can safely consider that $\Omega_{p1} \approx \Omega_{p2} = \Omega_p$. The probe pulses ($\Omega_{p1}$, Ω_{p2}) have different frequency (ω_{p1}, ω_{p2}) but they possess similar intensity, temporal profile and polarization.

We perform the following unitary transformation in order to remove the explicit time dependence from the Hamiltonian

$$H = U^{\dagger}H'U - i\hbar U^{\dagger}\frac{\partial U}{\partial t}, \tag{3}$$

where U is defined as

$$U = e^{-i(\omega_{p1}|1\rangle\langle 1| + (\omega_{p1}-\omega_c)|4\rangle\langle 4| + (\omega_{p1}-\omega_c+\omega_{p2})|2\rangle\langle 2|)t}. \tag{4}$$

Now the transformed Hamiltonian H takes the following form

$$\begin{aligned} H = &-\hbar\Delta_p|1\rangle\langle 1| - \hbar(\Delta_p - \Delta_c)|4\rangle\langle 4| \\ &- \hbar(\Delta_p - \Delta_c + \Delta_q)|2\rangle\langle 2| - \hbar\Omega_p|1\rangle\langle 3| \\ &- \hbar\Omega_c|1\rangle\langle 4| - \hbar\Omega_p|2\rangle\langle 4| + h.c., \end{aligned} \tag{5}$$

where $\Delta_p = \omega_{p1} - \omega_{13}$ and $\Delta_q = \omega_{p2} - \omega_{24}$ are the detunings of the probe field with $|1\rangle \leftrightarrow |3\rangle$ and $|2\rangle \leftrightarrow |4\rangle$ transitions, respectively. The detuning due to the control field corresponding to the $|1\rangle \leftrightarrow |4\rangle$ transition is given by $\Delta_c = \omega_c - \omega_{14}$.

2.2. Dynamic equations

We use Liouville's equation to account for the various radiative and non-radiative decay processes of the atomic system. The decay of the atomic system is caused by various mechanisms such as flight-through broadening, population exchange, and atom–atom and atom–wall collisions. To govern the response of the atomic populations and coherences of the four-level atomic system, the following density matrix equations are employed

$$\dot{\rho} = -\frac{i}{\hbar}[H, \rho] + \mathcal{L}_{\rho} \tag{6}$$

where the second term represents the decay processes that can be determined by

$$\mathcal{L}\rho = \mathcal{L}_r\rho + \mathcal{L}_c\rho \tag{7}$$

with

$$\mathcal{L}_r\rho = -\sum_{i=1}^{2}\sum_{j=3}^{4}\frac{\gamma_{ji}}{2}(|i\rangle\langle i|\rho - 2|j\rangle\langle j|\rho_{ii} + \rho|i\rangle\langle i|). \tag{8}$$

The spontaneous decay rates from the excited state $|i\rangle$, ($i \in 1, 2$) to the ground state $|j\rangle$, ($j \in 3, 4$) are denoted by γ_{ji} in equation (8). The dephasing in the ground state [$\mathcal{L}_c\rho$ in (7)] is due to collision at a rate γ_c. Now the dynamics of the model system can be obtained in the following form

$$\begin{aligned} \dot{\rho}_{11} &= -(\gamma_{31} + \gamma_{41})\rho_{11} + i\Omega_p\rho_{31} + i\Omega_c\rho_{41} - i\Omega_p^*\rho_{13} \\ &\quad - i\Omega_c^*\rho_{14}, \\ \dot{\rho}_{12} &= -\left[i(\Delta_q - \Delta_c) + \frac{1}{2}(\gamma_{31} + \gamma_{41} + \gamma_{32} + \gamma_{42})\right]\rho_{12} \\ &\quad + i\Omega_p\rho_{32} + i\Omega_c\rho_{42} - i\Omega_p^*\rho_{14}, \\ \dot{\rho}_{13} &= \left[i\Delta_p - \frac{1}{2}(\gamma_{31} + \gamma_{41})\right]\rho_{13} + i\Omega_p(\rho_{33} - \rho_{11}) \\ &\quad + i\,\Omega_c\rho_{43}, \\ \dot{\rho}_{14} &= \left[i\Delta_c - \frac{1}{2}(\gamma_{31} + \gamma_{41})\right]\rho_{14} + i\Omega_p(\rho_{34} - \rho_{12}) \\ &\quad + i\Omega_c(\rho_{44} - \rho_{11}), \\ \dot{\rho}_{22} &= -(\gamma_{32} + \gamma_{42})\rho_{22} + i\Omega_p\rho_{42} - i\Omega_p^*\rho_{24}, \\ \dot{\rho}_{23} &= \left[i(\Delta_p - \Delta_c + \Delta_q) - \frac{1}{2}(\gamma_{32} + \gamma_{42})\right]\rho_{23} \\ &\quad + i\Omega_p(\rho_{43} - \rho_{21}), \\ \dot{\rho}_{24} &= \left[i\Delta_q - \frac{1}{2}(\gamma_{32} + \gamma_{42})\right]\rho_{24} + i\Omega_p(\rho_{44} - \rho_{22}) \\ &\quad - i\Omega_c\rho_{21}, \\ \dot{\rho}_{33} &= \gamma_{31}\rho_{11} + \gamma_{32}\rho_{22} + i\Omega_p^*\rho_{13} - i\Omega_p\rho_{31} \\ \dot{\rho}_{34} &= -[i(\Delta_p - \Delta_c) + \gamma_c]\rho_{34} + i\Omega_p^*\rho_{14} - i\Omega_p\rho_{32} \\ &\quad - i\Omega_c\rho_{31}, \\ \dot{\rho}_{44} &= -(\dot{\rho}_{11} + \dot{\rho}_{22} + \dot{\rho}_{33}) \\ \dot{\rho}_{ij} &= \dot{\rho}_{ji}^* \end{aligned} \tag{9}$$

where the overdot stands for the time derivative and the star (*) denotes the complex conjugate. The atoms in the room-temperature vapor cell have random thermal motion and have a finite velocity associated with each. Due to the finite velocity, each atom experiences a different Doppler shift in laser field detuning, i.e. $\Delta' = \Delta \pm kv$, where the sign of frequency shift $\pm kv$ indicates the motion of atoms either counter-propagating or co-propagating. The presence of different Doppler shifts causes the atomic susceptibility to be inhomogeneously broadened. In the presence of the Doppler shift, the probe and control field detuning are modified to $\Delta_p' = \Delta_p - k_{p1}v$, $\Delta_q' = \Delta_q - k_{p2}v$, $\Delta_c' = \Delta_c - k_cv$, respectively. Therefore, these effects can be incorporated into the equations of motion (9) by taking into account the averaging over a Maxwell velocity distribution. Hence the velocity averaging of the atomic coherences $\langle\rho_{ij}(z, t)\rangle$ can be expressed as

$$\langle\rho_{ij}(z, t)\rangle = \int \rho_{ij}(z, v, t)\mathcal{P}(kv)d(kv), \tag{10}$$

where $\mathcal{P}(kv)d(kv)$ is the probability that an atom has a velocity between v and $v + dv$ and obeys the Maxwell–Boltzmann velocity distribution

$$\mathcal{P}(kv)d(kv) = \frac{1}{\sqrt{2\pi D^2}}e^{-\frac{(kv)^2}{2D^2}}d(kv). \tag{11}$$

The Doppler line width D is given by $D = \sqrt{k_BT\nu_c^2/Mc^2}$, where M is the atomic mass, k_B is the Boltzmann constant and

T is the thermal equilibrium temperature. At room temperature ($T = 300$ K), the Doppler width, D, is 37γ for ^{87}Rb atoms.

2.3. Pulse propagation equations

In this section, we use Maxwell's equations to govern the spatio-temporal evaluation of an optical field through a nonlinear medium. The wave equation for the probe, control and generated fields can be expressed as

$$\left(\nabla^2 - \frac{1}{c^2}\frac{\partial^2}{\partial t^2}\right)\vec{E} = \frac{4\pi}{c^2}\frac{\partial^2\vec{\mathcal{P}}}{\partial t^2}, \tag{12}$$

where $\vec{E} = \vec{E}_{p1} + \vec{E}_{p2} + \vec{E}_c + \vec{E}_g$ is the total field and its induced polarization is $\vec{\mathcal{P}}$. The source term $\vec{\mathcal{P}}$ that appears on the right-hand side of equation (12) is the origin of the linear and nonlinear response of the medium. The macroscopic polarization $\vec{\mathcal{P}}$ can be defined in terms of the atomic coherences as

$$\begin{aligned}\vec{\mathcal{P}} = \mathcal{N}(&\vec{d}_{13}\rho_{13}e^{-i\omega_{p1}t} + \vec{d}_{24}\rho_{24}e^{-i\omega_{p2}t} \\ &+ \vec{d}_{14}\rho_{14}e^{-i\omega_c t} + \vec{d}_{23}\rho_{23}e^{-i\omega_g t} + c.c.,)\end{aligned} \tag{13}$$

where $\mathcal{N}$ is the atomic density. Note that the atomic density under consideration is weak, otherwise local field correction needs to be taken into account. Under slowly-varying envelope approximation, equations (12) can be reformulated as

$$\left(\frac{\partial}{\partial z} + \frac{1}{c}\frac{\partial}{\partial t}\right)\Omega_p = i\eta\left\langle\frac{1}{3}\rho_{13}(z,t) + \frac{1}{4}\rho_{24}(z,t)\right\rangle, \tag{14}$$

$$\left(\frac{\partial}{\partial z} + \frac{1}{c}\frac{\partial}{\partial t}\right)\Omega_g = i\eta\left\langle\frac{1}{12}\rho_{23}(z,t)\right\rangle. \tag{15}$$

We neglect the propagation of the control field because its intensity is much higher than the probe and FWM signal intensity. The coupling constants for the probe and generated field are defined in terms of the reduced coupling constant, $\eta = 2\pi k\mathcal{N}|\vec{d}_{ij}^{\,R}|^2/\hbar$, as follows

$$\eta_{p1} = \frac{\eta}{3}; \quad \eta_{p2} = \frac{\eta}{4}; \quad \eta_g = \frac{\eta}{12} \tag{16}$$

where $|\vec{d}_{ij}^{\,R}|$ is the reduced matrix element. The spontaneous decay rates from the excited states into the ground states are also modified due to the different coupling strength and can be written as

$$\gamma_{31} = \frac{\gamma}{3}; \quad \gamma_{41} = \frac{\gamma}{4}; \quad \gamma_{32} = \frac{\gamma}{12}; \quad \gamma_{42} = \frac{\gamma}{4} \tag{17}$$

where the reduced spontaneous decay rate is defined as $\gamma = 4|\vec{d}_{ij}^{\,R}|^2k^3/3\hbar$. The angular bracket denotes a statistical average over the velocity distribution of the atom. We introduce the following co-moving coordinate system in order to perform numerical computation:

$$\tau = t - \frac{z}{c}, \quad \xi = z. \tag{18}$$

Therefore, the expressions within the round bracket of equation (14) can be easily substituted by $\partial/\partial\,\xi$ in the frame of the moving coordinate system. Subsequently, simultaneous solutions of the Bloch equation (9) and Maxwell's equation (14) in space-time coordinates explore the dynamical progression of the optical fields inside the medium.

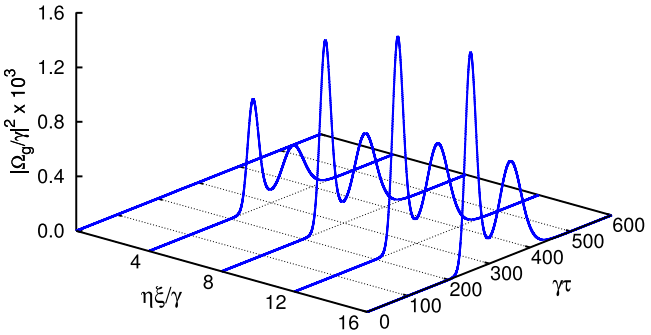

Figure 2. Propagation dynamics of the generated FWM signal as a function of position and time. The parameters are $\Omega_p^0 = 0.3\gamma$, $\Omega_c^0 = 3.0\gamma$, $\mathcal{N} = 4 \times 10^{10}$ atoms cm^{-3}, $\lambda = 7.95 \times 10^{-5}$ cm, $\Delta_p = \Delta_c = \Delta_q = \Delta_g = 0$, $\sigma_1 = 30/\gamma$, $\sigma_2 = 50/\gamma$, $\gamma\tau_1 = 250$, $\gamma\tau_2 = 350$, $D = 37\gamma$, T = 300 K, $\gamma_c \approx 1 \times 10^3$ Hz.

3. Generation and control of FWM signal

In this section, we proceed with the numerical simulation of Maxwell–Bloch equations to reveal the generation of the optical field and its control by exploiting the FWM mechanism. We have adopted the Cash–Karp Runge–Kutta method in order to solve coupled partial differential equations. We begin with a complicated shaped input probe pulse which is a combination of a Gaussian and secant hyperbolic pulse having different widths ($\sigma_1 = 30/\gamma$, $\sigma_2 = 50/\gamma$). The time-dependent envelope of the probe field at the entry face of the medium can be written as

$$\Omega_p(\xi = 0, \tau) = \Omega_p^0\left[e^{-\left(\frac{\tau-\tau_1}{\sigma_1}\right)^2} + sech\left(\frac{\tau - \tau_2}{\sigma_2}\right)\right] \tag{19}$$

where Ω_p^0, σ_i, $i \in \{1, 2\}$ and τ_i, $i \in \{1, 2\}$ are the amplitude, temporal width and peak location of the complicated shaped probe field, respectively. In our entire computation, we have assumed that the amplitude of the control field ($\Omega_c^0 = 3.0\gamma$) is larger than the amplitude of the probe field ($\Omega_p^0 = 0.3\gamma$) and subsequently the dynamical evolution of the control field can be neglected. Initially all atoms are occupied in the $|3\rangle$ state whereas all other states are unoccupied for $\xi \in (0, L)$.

Our first finding on the generation of the optical pulse in the presence of a continuous-wave (cw) control field is shown in figure 2. Figure 2 shows the temporal variation of the generated field at different propagation distances. It is clear from figure 2 that the amplitude of the generated field increases gradually and takes the probe field shape while propagating along the medium. Note that the temporal shape of the generated field remains unchanged after it attains saturation intensity. For the sake of generality, we compare the temporal shape of the generated field with the probe field as in figure 3. It can be seen that the time-dependent envelope of the generated field is the same as the input probe field,

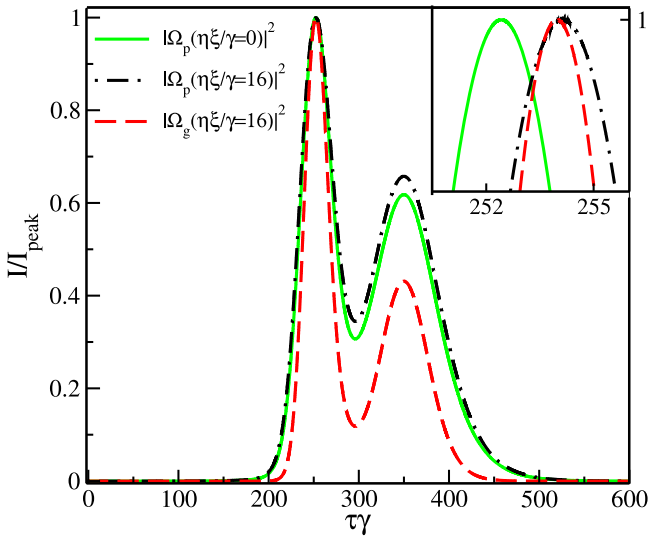

Figure 3. Normalized intensity profile, I/I_{peak}, of the complicated shaped probe pulse and FWM signal at input ($\eta\xi/\gamma = 0$) and output ($\eta\xi/\gamma = 16$) boundary of the medium. Temporal peak position of the output pulses is shifted at $\gamma\tau = 252.5$. Inset figure shows the actual peak location. All other parameters are the same as in figure 2.

except its width is a scaled version of the probe pulse. We also notice that the temporal shapes of both generated and probe fields propagate through the medium without absorption and distortion. Therefore, only the cw control field efficiently acquires the temporal shape of the probe field to generate signals and protect them during propagation.

Further, we have calculated the efficiency of the FWM process, η_{eff} as a ratio of the energy of the output FWM-generated field and energy of the input probe field [46]

$$\eta_{eff} = \frac{\int_{-\infty}^{\infty} |\vec{E}_g(z = L, \tau)|^2 \, d\tau}{\int_{-\infty}^{\infty} \sum_{i=1}^{2} |\vec{E}_{pi}(z = 0, \tau)|^2 \, d\tau}; \tag{20}$$

$$|\vec{E}_g|^2 = \frac{\hbar^2 |\Omega_g|^2}{|\vec{d}_{23}|^2}; \quad |\vec{E}_{pi}|^2 = \frac{\hbar^2 |\Omega_p|^2}{|\vec{d}_{13}|^2} \tag{21}$$

The efficiency of the FWM process, η_{eff}, is 2.8%. The efficiency also depends on the control field intensity and can be enhanced further by reducing the control field intensity as shown in figure 4 in the manuscript. However, the line width of the EIT window also depends on Ω_c and can be expressed as $(\Delta\omega)_{EIT} \propto |\Omega_c|^2/\gamma$ [47], which limits the FWM efficiency. This limitation can be avoided by considering a suitable spectral width of the probe pulse.

In order to prove the robustness of the model system, we next consider the input probe field to be an amplitude-modulated Gaussian pulse. For this purpose, the input envelope for the probe field is expressed as follows

$$\Omega_p(\xi = 0, \tau) = \Omega_p^0(1 + m_a \cos \omega_m t) e^{-\left(\frac{\tau - \tau_0}{\sigma_p}\right)^2} \tag{22}$$

where m_a and ω_m are termed as the depth of modulation and frequency of the modulating signal, respectively. In practice, ω_m is small compared to the carrier frequency ω_p of the probe pulse. Figure 5 depicts the intensity profile of the probe and generated fields as a function of $\gamma\tau$ at the propagation distance

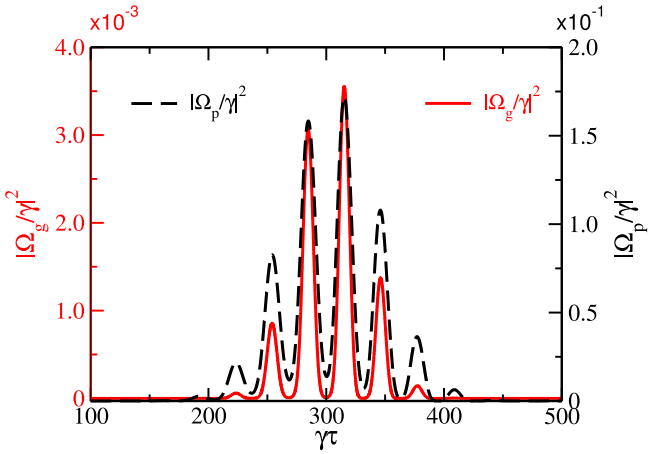

Figure 4. Imaginary part of nonlinear Doppler-averaged coherence, $\langle\rho_{23}\rangle$, as a function of Δ_p in units of γ for various values of Ω_c. The parameters are $\Omega_p^0 = 0.3\gamma$, $\Omega_c^0 = 3.0\gamma$, $\Delta_c = \Delta_q = 0$, $D = 37\gamma$, T = 300 K, $\gamma_c \approx 1 \times 10^3$ Hz, $\gamma = 5.746 \times 10^6$ Hz.

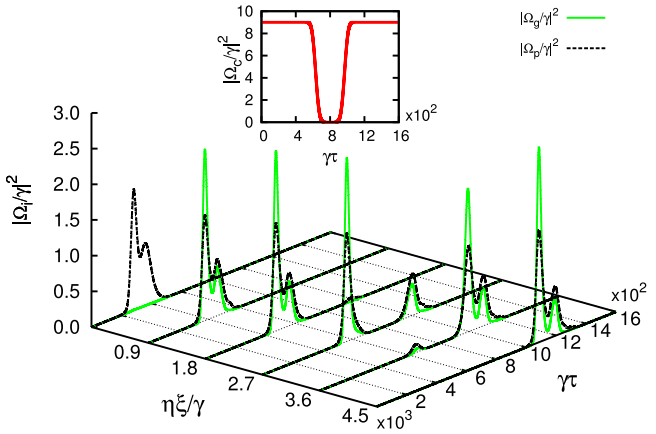

Figure 5. Intensity profile of the amplitude-modulated Gaussian-shaped probe pulse and generated FWM signal at output ($\eta\xi/\gamma = 16$) boundary of the medium. The parameters for the probe pulse are $\Omega_p^0 = 0.3\gamma$, $m_a = 0.65$, $w_m = \gamma/5$, $\sigma_p = 75/\gamma$ and $\gamma\tau_0 = 300$. Other parameters are the same as in figure 2.

$\eta\xi/\gamma = 16$. This figure confirms precisely that the generated FWM signal gets its shape from the envelope of the probe field and propagates as a shape-preserving pulse. However, the time resolution of the generated amplitude-modulated pulse is higher compared to the probe pulse.

4. Storage and retrieval of electromagnetic radiation

In the previous section, we demonstrated how the time-independent control field efficiently generates and controls the propagation of the FWM signal. Here we explore the dynamics of the generated field in the presence of the time-dependent profile of the control field. We address this issue by considering the temporal profile of the control field to be of inverted super-Gaussian shape, which is defined as

$$\Omega_c(\xi = 0, \tau) = \Omega_c^0[1 - e^{-\left(\frac{\tau - \tau_c}{\sigma_c}\right)^{\alpha}}], \tag{23}$$

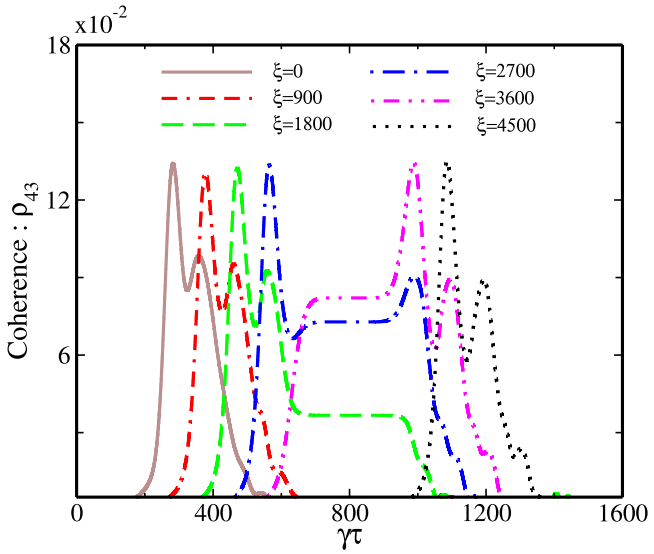

Figure 6. Storage and retrieval of complicated shaped probe pulse (dashed black line, $i = p$) and generated FWM signal (solid green line, $i = g$) are demonstrated. We multiply 10^1 and 10^3 with the probe field intensity ($|\Omega_p/\gamma|^2$) and FWM signal intensity ($|\Omega_g/\gamma|^2$), respectively. Inset figure shows intensity profile of the control field (solid red). The parameters are $\sigma_1 = 30/\gamma$, $\sigma_2 = 50/\gamma$, $\gamma\tau_1 = 280$, $\gamma\tau_2 = 360$, $\sigma_c = 160/\gamma$, $\gamma\tau_c = 800$, $\alpha = 4$ and all other parameters are the same as in figure 2.

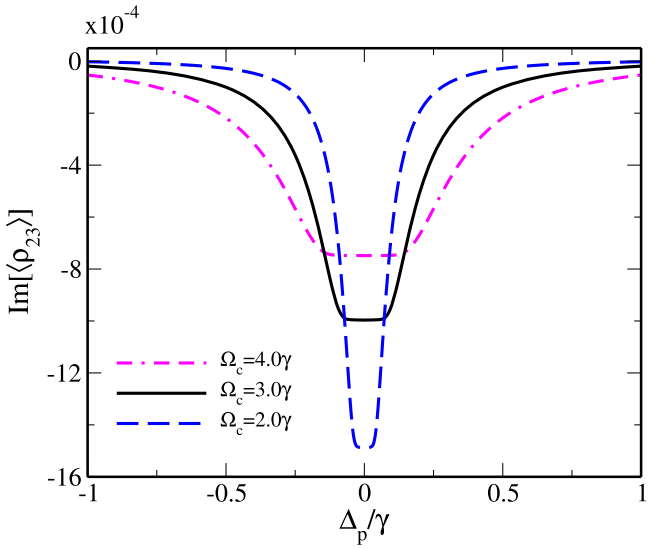

Figure 7. The temporal profile of ground-state atomic coherence, ρ_{43}, is plotted as a function of time for different propagation distances. All parameters are the same as in figure 6.

where the parameter α regulates the rapidity of the switching action of the control field as shown in the inset of figure 6. The switching off and on of the control field intensity in the time domain holds the key to the storage and retrieval process. Figure 6 displays the spatio-temporal characteristics of the probe and FWM fields. The initial profile of the probe field is chosen as a combination of Gaussian and secant hyperbolic pulse having different widths. As seen from figure 6 the probe field intensity gradually diminishes due to the dynamical reduction of the control intensity. Simultaneously, the FWM signal is formed and its spatio-temporal evolution follows the same dynamical behavior as the probe field.

The control field not only generates the FWM signal but also enables the storage and retrieval of the signal along with the probe pulse by temporal variation of its own intensity. The intensity lowering (rising) to zero (maximum) with time produces switching off (on) of the control field as shown in the inset of figure 6. The spatio-temporal evolution of the probe and generated signals in the presence of the super-Gaussian-shaped control field is shown in figure 6. The signal and probe fields are depicted by the solid green and dashed black lines, respectively. Figure 6 shows that the generation of the signal field is accomplished within a short length of medium in the presence of both the control and probe fields. It is also evident from figure 6 that storage of the signal and probe fields starts as soon as both peaks experience the falling intensity of the control field. Hence the intensities of both the signal and probe fields are gradually stored by adiabatic switching of the control field during the propagation through the atomic medium. The storing of the fields can be completed by making the intensity of the control field zero. The stored pulses can be retrieved on demand by switching on the control field. The retrieval process of the stored fields can be initiated by switching on the control field at a later time. The maximum intensity of the control field leads to retrieval of both the probe and signal from the medium without loss of generality.

Next we investigate the ground-state atomic coherence which is solely responsible for the storage and retrieval of electromagnetic radiation in an atomic medium [48]. Subsequently we have plotted the atomic coherence ρ_{43} as a function of time at different propagation distances as shown in figure 7. As depicted from figure 7, at the entry face of the medium, $\eta\xi/\gamma = 0$, ρ_{43} takes the temporal shape of the probe field in the presence of constant control. The atomic coherence attains its maximum value when control field is switched off. The probe and signal pulses are stored inside the medium in the form of ground atomic coherence by switching off the control field. This coherence (ρ_{43}) is well preserved inside the medium and can be retrieved efficiently before it decays at a rate of γ_c. The atomic coherence starts generating the replica of the stored pulses after the control field is switched on. The Raman scattering between the stored atomic coherence and control field intensity produces the stored signal again. Therefore, the atomic coherence plays the main role in the storage and retrieval of the probe as well as the FWM signal.

5. Analysis and discussions

5.1. Perturbative analysis

In this section, we derive an analytical expression for the atomic coherence which can successfully explain the generation of the signal due to four-wave mixing in the four-level atomic system. The perturbative expression for the coherence and population is determined under weak probe approximation ($\Omega_p < \Omega_c$) that is correct in all orders for the control field of

Rabi frequencies Ω_c and second order in probe Rabi frequencies Ω_p. The solutions of the density matrix equations can be approximated as

$$\rho_{ij} = \rho_{ij}^{(0)} + \Omega_p \rho_{ij}^{(1)} + \Omega_p^* \rho_{ij}^{(2)} + \Omega_p^2 \rho_{ij}^{(3)} + |\Omega_p|^2 \rho_{ij}^{(4)} + \Omega_p^{*2} \rho_{ij}^{(5)} \tag{24}$$

where $\rho_{ij}^{(0)}$ describes the solution in the absence of Ω_p and $\rho_{ij}^{(k)}$, $k \in \{1, 2, 3, 4, 5\}$ is the higher-order solution in the presence of weak Ω_p. The steady-state value of the atomic coherence, ρ_{23}, can be expressed by the following expression

$$\rho_{23} = \frac{i\Omega_p^2 \Omega_c^*}{\Gamma_1 \Gamma_3 [\Gamma_2 + \frac{\Omega_c^2}{\Gamma_1}]}, \tag{25}$$

where

$$\begin{aligned} \Gamma_1 &= i\Delta_p - \frac{\gamma_{31} + \gamma_{41}}{2}, \\ \Gamma_2 &= i(\Delta_p - \Delta_c) - \gamma_c, \\ \Gamma_3 &= i(\Delta_p - \Delta_c + \Delta_q) - \frac{\gamma_{32} + \gamma_{42}}{2}. \end{aligned} \tag{26}$$

The above expression corresponds to four-wave mixing in a system of four level atoms and produces a frequency $\omega_g = \omega_{p1} - \omega_c + \omega_{p2}$. The induced nonlinear atomic polarization $\vec{P}^{NL}$ is expressed as $\vec{P}^{NL} = \chi^{(3)}(\omega_g)\vec{E}_{p1}\vec{E}_c^*\vec{E}_{p2}$ where $\chi^{(3)}(\omega_g)$ is a third-order nonlinearity. Under Doppler broadening, the nonlinear susceptibility $\chi^{(3)}(\omega_g)$ can be written as

$$\langle \chi^{(3)}(\omega_g) \rangle = \frac{\mathcal{N}|\vec{d}_{23}||\vec{d}_{13}|^2|\vec{d}_{14}|}{\hbar^3 |\Omega_p|^2 \Omega_c^*} \langle \rho_{23} \rangle, \tag{27}$$

where $\mathcal{N}$ is the atomic density.

5.2. Nonlinear susceptibility

We next study the nonlinear susceptibility of the medium and its variation with the control field intensity. We use the weak-approximated analytical solution (25) to obtain the response of the generated signal coherence as shown in figure 4. The plots in figure 4 show gain which ensures that new optical field generation is possible even in the weak probe regime. The gain of the generated signal can be enhanced by reducing the control field intensity as clearly shown in figure 4 with the double dash-dotted magenta curve ($\Omega_c = 4.0\gamma$), solid black curve ($\Omega_c = 3.0\gamma$) and dashed blue curve ($\Omega_c = 2.0\gamma$). The condition of the stable dark state, i.e. $\Omega_p < \Omega_c$, becomes feeble as the control field intensity is reduced significantly, and causes the population to leave the dark state $|3\rangle$ and populate the excited states $|1\rangle$ and $|2\rangle$, which enhances the gain of the FWM signal. Simultaneously, the probe pulse suffers absorption and distortion due to the narrowness of the medium transmission window at low control field intensity because $(\Delta\omega)_{EIT} \propto |\Omega_c|^2/\gamma$. However, the transmission and distortion of the probe pulse can be avoided by considering a suitable spectral width of the probe pulse so that the spectrum of the probe pulse will be well contained within the transparency window of the medium. Hence the efficiency of nonlinear signal generation can be enhanced with a suitable value of control field intensity.

6. Conclusion

In conclusion, we have demonstrated efficient generation and control of a non-degenerate FWM signal in an N-type inhomogeneously broadened atomic medium. A strong control field and two weak probe fields tailored the medium susceptibility with a gain profile which enabled us to generate the FWM signal. This scheme generates a scaled copy of the input probe pulse which travels through the atomic medium along with the probe field without changing its shape and intensity. We further study the propagation dynamics, storage and retrieval of the generated FWM signal in the nonlinear medium by considering a complicated combination of Gaussian and secant hyperbolic shape as well as an amplitude-modulated signal. These unique features have important applications in signal processing in optical communication as well as in quantum information science [49, 50].

Acknowledgments

N S M would like to thank MHRD, Government of India for financial support. T N D and N S M acknowledge the Science and Engineering Board of India for financial support (Grant No. CRG/2018/000054).

ORCID iDs

Nawaz Sarif Mallick https://orcid.org/0000-0001-9085-543X

References

[1] Fleischhauer M, Imamoglu A and Marangos J P 2005 *Rev. Mod. Phys.* **77** 633–73
[2] Agarwal G S 2012 *Coherent Control of the Optical Properties* (Cambridge University Press) pp 385–412
[3] Hamedi H R, Ruseckas J and Juzeliūnas G 2017 *J. Phys. B: At. Mol. Opt. Phys.* **50** 185401
[4] Liu R, Liu T, Wang Y, Li Y and Gai B 2017 *Phys. Rev.* A **96** 053823
[5] Arsenovic D, Curcic M M, Khalifa T, Zlatkovic B, Nikitovic Z, Radojicic I S, Krmpot A J and Jelenkovic B M 2018 *Phys. Rev.* A **98** 023829
[6] Patnaik A K, Kien F L and Hakuta K 2004 *Phys. Rev.* A **69** 035803
[7] Nakao H and Yamamoto N 2017 *J. Phys. B: At. Mol. Opt. Phys.* **50** 065501
[8] Zhang R and Wang X B 2016 *Phys. Rev.* A **94** 063856
[9] Katz O and Firstenberg O 2018 *Nat. Commun.* **9** 2074
[10] Firstenberg O, Adams C S and Hofferberth S 2016 *J. Phys. B: At. Mol. Opt. Phys.* **49** 152003
[11] Dey T N and Evers J 2011 *Phys. Rev.* A **84** 043842
[12] Cui N, Gan Z and Zhang L 2017 *Sci. Rep.* **7** 14198
[13] Radwell N, Clark T W, Piccirillo B, Barnett S M and Franke-Arnold S 2015 *Phys. Rev. Lett.* **114** 123603
[14] Sharma S and Dey T N 2017 *Phys. Rev.* A **96** 033811
[15] Hamedi H R and Juzeliunas G 2015 *Phys. Rev.* A **91** 053823
[16] Mallick N S, Dey T N and Pandey K 2017 *J. Phys. B: At. Mol. Opt. Phys.* **50** 195502

[17] Béjot P and Kasparian J 2018 *Phys. Rev.* A **97** 063835
[18] Sun H, Niu Y, Jin S and Gong S 2007 *J. Phys. B: At. Mol. Opt. Phys.* **40** 3037
[19] Dmochowski G, Feizpour A, Hallaji M, Zhuang C, Hayat A and Steinberg A M 2016 *Phys. Rev. Lett.* **116** 173002
[20] de Oliveira F A M, de Araújo C B and Rios Leite J R 1988 *Phys. Rev.* A **38** 5688–97
[21] Lopez J P, Moreno M P, de Miranda M H G and Vianna S S 2017 *J. Phys. B: At. Mol. Opt. Phys.* **50** 085001
[22] Akulshin A M, Orel A A and McLean R J 2011 *J. Phys. B: At. Mol. Opt. Phys.* **45** 015401
[23] Jeong T and Moon H S 2016 *Opt. Express* **24** 28774–83
[24] Ham B S and Hemmer P R 2000 *Phys. Rev. Lett.* **84** 4080–3
[25] Kölle A, Epple G, Kübler H, Löw R and Pfau T 2012 *Phys. Rev.* A **85** 063821
[26] Lee C Y, Wu B H, Wang G, Chen Y F, Chen Y C and Yu I A 2016 *Opt. Express* **24** 1008–16
[27] Liu Z Y, Xiao J T, Lin J K, Wu J J, Juo J Y, Cheng C Y and Chen Y F 2017 *Sci. Rep.* **7** 15796
[28] Juo J Y, Lin J K, Cheng C Y, Liu Z Y, Yu I A and Chen Y F 2018 *Phys. Rev.* A **97** 053815
[29] Li H C, Ge G Q and Zubairy M S 2018 *Phys. Rev.* A **97** 053826
[30] Braje D A, Balić V, Goda S, Yin G Y and Harris S E 2004 *Phys. Rev. Lett.* **93** 183601
[31] Kang H, Hernandez G and Zhu Y 2004 *Phys. Rev.* A **70** 061804
[32] Sahoo S S, Bhowmick A and Mohapatra A K 2017 *J. Phys. B: At. Mol. Opt. Phys.* **50** 055501
[33] Zhang Y, Brown A W, Gan C and Xiao M 2007 *J. Phys. B: At. Mol. Opt. Phys.* **40** 3319–29
[34] Kang H, Hernandez G and Zhu Y 2004 *Phys. Rev. Lett.* **93** 073601
[35] Chiu C K, Chen Y H, Chen Y C, Yu I A, Chen Y C and Chen Y F 2014 *Phys. Rev.* A **89** 023839
[36] Li J B, He M D and Chen L Q 2014 *Opt. Express* **22** 24734–41
[37] Li J B, Xiao S, Liang S, He M D, Luo J H, Kim N C and Chen L Q 2017 *Opt. Express* **25** 25663–73
[38] Camacho R M, Vudyasetu P K and Howell J C 2009 *Nat. Photon.* **3** 103–6
[39] Raczynski A and Zaremba J 2002 *Opt. Commun.* **209** 149–54
[40] Phillips N B, Gorshkov A V and Novikova I 2011 *Phys. Rev.* A **83** 063823
[41] Wu J, Liu Y, Ding D S, Zhou Z Y, Shi B S and Guo G C 2013 *Phys. Rev.* A **87** 013845
[42] Hosseini M, Sparkes B M, Campbell G T, Lam P K and Buchler B C 2012 *J. Phys. B: At. Mol. Opt. Phys.* **45** 124004
[43] Xu D, Hang C and Huang G 2018 *Phys. Rev.* A **98** 043848
[44] Lauk N, O'Brien C and Fleischhauer M 2013 *Phys. Rev.* A **88** 013823
[45] Phillips N B, Novikova I, Mikhailov E E, Budker D and Rochester S 2013 *J. Mod. Opt.* **60** 64–72
[46] Wu Y and Yang X 2004 *Phys. Rev.* A **70** 053818
[47] Fleischhauer M and Lukin M D 2002 *Phys. Rev.* A **65** 022314
[48] Fleischhauer M and Lukin M D 2000 *Phys. Rev. Lett.* **84** 5094–7
[49] Cai Y, Feng J, Wang H, Ferrini G, Xu X, Jing J and Treps N 2015 *Phys. Rev.* A **91** 013843
[50] Wang H, Fabre C and Jing J 2017 *Phys. Rev.* A **95** 051802